



# Electron Cryomicroscopic Visualization of PomA/B Stator Units of the Sodium-driven Flagellar Motor in Liposomes

Koji Yonekura<sup>1,2\*</sup>, Toshiharu Yakushi<sup>3</sup>, Tatsuo Atsumi<sup>3</sup>  
Saori Maki-Yonekura<sup>2</sup>, Michio Homma<sup>3</sup> and Keiichi Namba<sup>1,2</sup>

<sup>1</sup>Graduate School of Frontier Biosciences, Osaka University 1-3, Yamadaoka, Suita, Osaka 565-0871, Japan

<sup>2</sup>Dynamic NanoMachine Project, ICORP, JST, 1-3, Yamadaoka, Suita, Osaka 565-0871, Japan

<sup>3</sup>Division of Biological Science Graduate School of Science Nagoya University, Chikusa-ku Nagoya 464-8602, Japan

A motor protein complex of the bacterial flagellum, PomA/B from *Vibrio alginolyticus*, was reconstituted into liposomes and visualized by electron cryomicroscopy. PomA/B is a sodium channel, composed of two membrane proteins, PomA and PomB, and converts ion flux to the rotation of the flagellar motor. *Escherichia coli* and *Salmonella* have a homolog called MotA/B, which utilizes proton instead of sodium ion. PomB and MotB have a peptidoglycan-binding motif in their C-terminal region, and therefore PomA/B and MotA/B are regarded as the stator. Energy filtering electron cryomicroscopy enhanced the image contrast of the proteins reconstituted into liposomes and showed that two extramembrane domains with clearly different sizes stick out of the lipid bilayers on opposite sides. Image analysis combined with gold labeling and deletion of the peptidoglycan-binding motif revealed that the longer one, ~70 Å long, is likely to correspond to the periplasmic domain, and the other, about half size, to the cytoplasmic domain.

© 2005 Elsevier Ltd. All rights reserved.

**Keywords:** bacterial flagellum; flagellar motor; stator; liposome; energy filtering electron cryomicroscopy

\*Corresponding author

## Introduction

The bacterial flagellum is a large macromolecular complex, composed of about 25 different proteins. It is used for bacterial motility by rotating the flagellar filaments, which grow to 10–15 µm long. The rotary motor at the base of the filament drives its rotation. The motor structure called the flagellar basal body crosses both the cytoplasmic and outer membrane and continues to the extracellular structure called the hook and the filament.<sup>1–4</sup> The motor is powered by the electrochemical potential of specific ions

across the cytoplasmic membrane. Genetic and physiological studies of the proton driven motors of *Escherichia coli* and *Salmonella typhimurium* have shown that two membrane proteins, MotA and MotB, form a complex responsible for torque generation<sup>5–8</sup> and presumably form a proton channel.<sup>9–11</sup> MotA and MotB have four and one transmembrane helices, respectively. The MotA/B complex also functions as the stator by being anchored to the peptidoglycan layer of the cell through a binding motif in the periplasmic domain of MotB.<sup>12,13</sup> Electron micrographs of freeze-fractured samples showed that the stator complexes appear as a circular array of particles on the cytoplasmic membrane, surrounding the rotor.<sup>14,15</sup> For torque generation, MotA/B is thought to undergo a conformational change coupled to the proton flux while it interacts with FliG, which is a component of the rotor and the motor switch complex. The switch complex, which is made of three proteins, FliG, FliM and FliN, forms the C-ring (Figure 1(a)), and is required for torque generation and regulation of the switching probability of the rotation direction of the motor.<sup>16–18</sup>

Present addresses: K. Yonekura and S. Maki-Yonekura, The W. M. Keck Advanced Microscopy Laboratory, Department of Biochemistry and Biophysics, University of California, San Francisco, 1700, 4th Street, San Francisco, CA 94143-2532, USA. T. Yakushi, Department of Bioscience and Biotechnology, Faculty of Agriculture, Shinshu University, Minamiminowa, Nagano 399-4598, Japan.

Abbreviations used: LDL, low-density lipoprotein; CTF, contrast transfer function.

E-mail address of the corresponding author: yone@msg.ucsf.edu

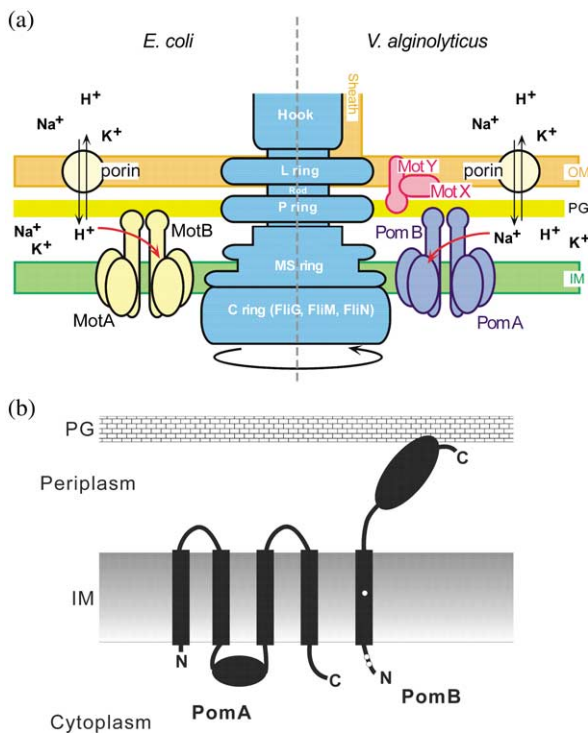


**Figure 1.** Schematic diagrams of two types of flagellar motors and membrane topology of PomA and PomB. (a) A hypothetical model for the proton-driven motor in *E. coli* and *Salmonella* (left) and the sodium-driven motor in *V. alginolyticus* (right). The sodium-driven polar flagellum of *Vibrio* is sheathed. The energy source for the flagellar motor rotation is provided by an electrochemical potential gradient across the inner membrane. Hypothetical functional units of the stator are  $(MotA)_4$ – $(MotB)_2$  and  $(PomA)_4(PomB)_2$ .<sup>33–36</sup> MotX and MotY colocalize to the outer membrane and interact with PomA/B.<sup>28,29</sup> IM, inner membrane; PG, peptidoglycan; OM, outer membrane. (b) Predicted membrane topology of PomA and PomB. Black columns within the inner membrane represent the transmembrane regions. Small white open circles in PomB indicate the positions of three cysteine residues (Cys8, Cys10 and Cys31). Large extramembrane domains are represented by ellipsoids.

Some bacteria, such as alkalophilic *Bacillus* and *Vibrio* species use the electrochemical potential of sodium ions to generate torque.<sup>19,20</sup> In *Vibrio*, such as *Vibrio alginolyticus*, *Vibrio parahaemolyticus*, and *Vibrio cholerae*,<sup>19,20</sup> which normally have only one flagellum at their cellular pole, four proteins, PomA, PomB, MotX, and MotY, have been identified and shown to be necessary for the rotation of the polar flagellar motor. The maximum rotational speed of the sodium-driven motor in *V. alginolyticus* is  $\sim 1700$  Hz,<sup>21</sup> while that of the proton-driven motor in *E. coli* is  $\sim 300$  Hz.<sup>22,23</sup> PomA and PomB are homologous to MotA and MotB, respectively, whereas paralogs of MotX and MotY<sup>24–27</sup> are not found in *E. coli*. Although the functions of MotX and MotY are not yet clear, recent studies show that they are located in the outer membrane and interact with the PomA/B complex.<sup>28,29</sup> PomA and PomB are thought to form a sodium channel complex.

Channel blockers for mammalian epithelial sodium ion channels such as amiloride and phenamil specifically inhibit the rotation of the sodium-type motor.<sup>30,31</sup> MotA/B from *E. coli* can drive the polar flagellum of *V. cholerae*<sup>26</sup> and *V. alginolyticus*<sup>32</sup> by proton motive force. Also, a complex of PomA and a chimera protein made of PomB and MotB segments can convert a proton-driven motor into a sodium-driven one.<sup>32</sup> Hence, PomA/B or MotA/B determines ion specificity of the motor, and the two types of motors must share a similar mechanism for ion-driven torque generation. Several studies suggested that the functional unit is  $(PomA)_4(PomB)_2$  or  $(MotA)_4(MotB)_2$ .<sup>33–36</sup> Figure 1 shows a schematic drawing of the proton-type motor in *E. coli* and *Salmonella* and the sodium-type motor in *Vibrio* and a topology diagram of the PomA/B complex.

Despite the importance of its function, the structural information of the stator complex is very limited and observation of the structure has not been reported to date except for the freeze-fracture views.<sup>14,15</sup> Here, we report the observation of a purified PomA/B complex reconstituted into liposomes by energy filtering electron cryomicroscopy. The image showed that two extramembrane domains stick out of the lipid bilayers on both sides but asymmetrically in size. Image analysis combined with gold labeling and deletion of the peptidoglycan-binding motif allowed domain assignment of the complex.

## Results

### Sample preparation

The purification protocol was changed from the previous one,<sup>37</sup> and Chaps, instead of sucrose monooctate, was used to solubilize the PomA/B complex, because Chaps was able to keep the complex more stably (T.A. *et al.*, unpublished results). Gel-filtration gave a clear single peak at 550 kDa as calibrated with soluble globular proteins used as standards. This indicates that PomA/B forms a large complex, but smaller than that formed in sucrose monooctate (900 kDa).<sup>37</sup> SDS-PAGE and immunoblots revealed that PomA forms a stable dimer that is resistant to SDS (the second and fifth lane in Figure 2).<sup>38</sup> The dimer band disappeared when the sample solution was dialyzed against non-detergent buffer solutions for a few days to reconstitute PomA/B into liposomes as shown in the third and sixth lane in Figure 2. Therefore, the dimer formation might be caused by the detergent Chaps.

We first observed negatively stained samples of purified PomA/B dissolved in detergent solutions by electron microscopy, but found only aggregation of the proteins. We also examined the same samples quickly frozen and embedded in vitreous ice, but we could not see any structure, presumably because the size of the predicted functional unit  $(PomA)_4(PomB)_2$ , of which the molecular mass is

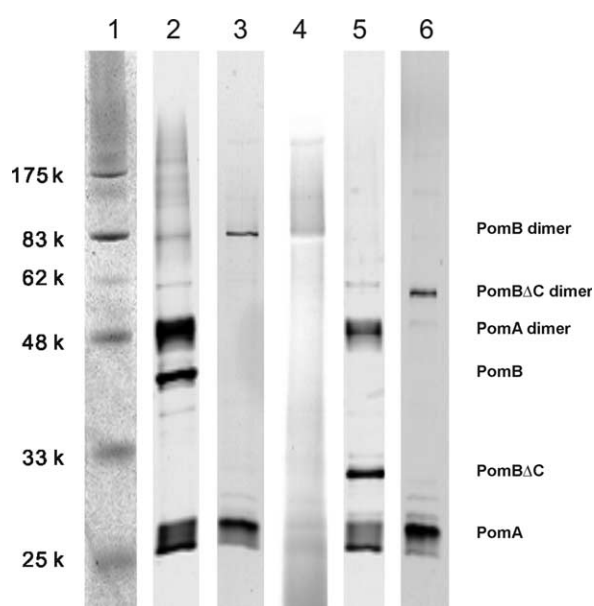


**Figure 2.** SDS-PAGE patterns of the purified PomA/B complex by silver staining. Lanes: 1, marker; 2, PomA/B; 3, PomA/B with bound Nanogold after reconstitution into liposomes with no reducing agent; 4, the same as lane 3 except that this was developed with a gold staining kit; 5, PomA/B $\Delta$ C,<sup>43</sup> the complex of PomA and a truncation variant of PomB missing the C-terminal 120 residues; and 6, PomA/B $\Delta$ C after reconstitution into liposomes with no reducing agent. Note that the bands of the PomA dimer disappear and the bands of PomB and PomB $\Delta$ C are replaced by those of their dimers, respectively, in lanes 3 and 6. The band of the PomA monomer moved faster than that of the PomB $\Delta$ C monomer despite that the molecular mass of PomA is larger.

170 kDa,<sup>33–36</sup> may be too small to visualize by electron cryomicroscopy when the complex is dispersed in solution. Also, visualization of the membrane-spanning structure of the complex would be more desirable. Therefore, reconstitution of the complex into liposomes was tried. After

testing various conditions for reconstitution into unilamellar liposomes with sizes suitable for electron cryomicroscopic observation, the protocol described in Materials and Methods, Sample preparation, gave good and reproducible results.

### Electron cryomicroscopy of proteoliposomes

We examined proteoliposomes by electron energy filtering microscopy, which can produce the image formed by zero-energy loss (zero-loss) electrons by removing inelastically scattered electrons, which contribute to noises in image formation. Most of the unilamellar liposomes prepared as described above had the size range from a few hundreds to a few thousands Å in diameter. Zero-loss images resolved the proteoliposomes significantly clearer than conventional electron cryomicrographs due to reduced noise and increased amplitude contrast.<sup>39–41</sup> This effect was more remarkable for larger liposomes because they are embedded in thicker ice. The phosphate head group of lipids in the lipid bilayers showed the highest contrast in the images even without energy filtering, but the contrast enhancement by zero-loss imaging was also most prominent, probably because phosphorus scatters more electrons inelastically than hydrogen, carbon, nitrogen and oxygen, and energy filtering can eliminate those electrons (Figure 3).

The purified PomA/B complex was reconstituted into liposomes by removal of the detergent by dialysis and quickly frozen for electron cryomicroscopic observation. There were aggregations, probably derived from PomA/B, but we found in many liposomes rod-shaped objects sticking out of the lipid bilayer plane on both sides (Figure 3). These two extramembrane domains were asymmetric in length but had a similar diameter of  $\sim 20$  Å. The longer one was  $\sim 70$  Å long and the shorter one was approximately one-half of it. There seemed to be no preferred orientations for insertion of the complex (Figure 4(a)). Although the orientation was different

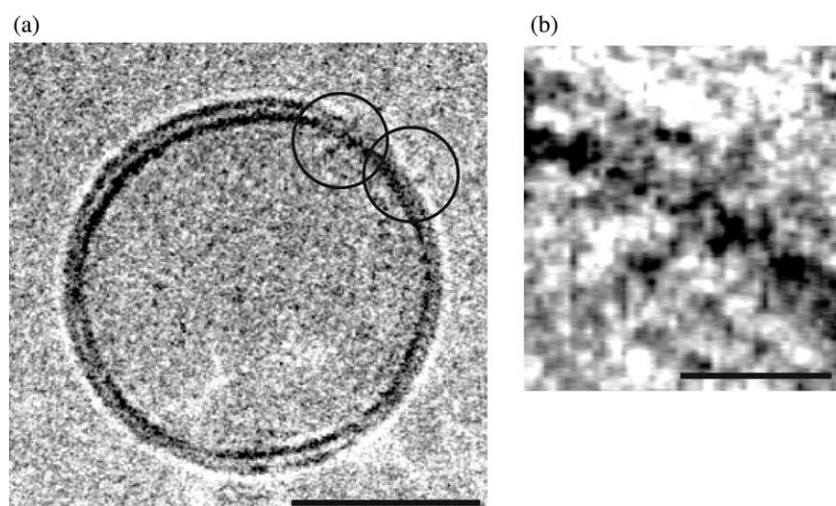


**Figure 3.** Zero-loss image of a PomA/B proteoliposome. (a) Typical electron cryomicrograph of a unilamellar proteoliposome with a diameter of  $\sim 1000$  Å. The lipid bilayers are clearly visible. Circles enclose elongated particles sticking out of the vesicle surface. The bar represents 500 Å. (b) Zoom-up view of the particle encircled in the upper left circle in (a). These images clearly show that two extramembrane domains of distinctly different sizes stick out of the lipid bilayers on both sides. The longer one is  $\sim 70$  Å long. The bar represents 100 Å.

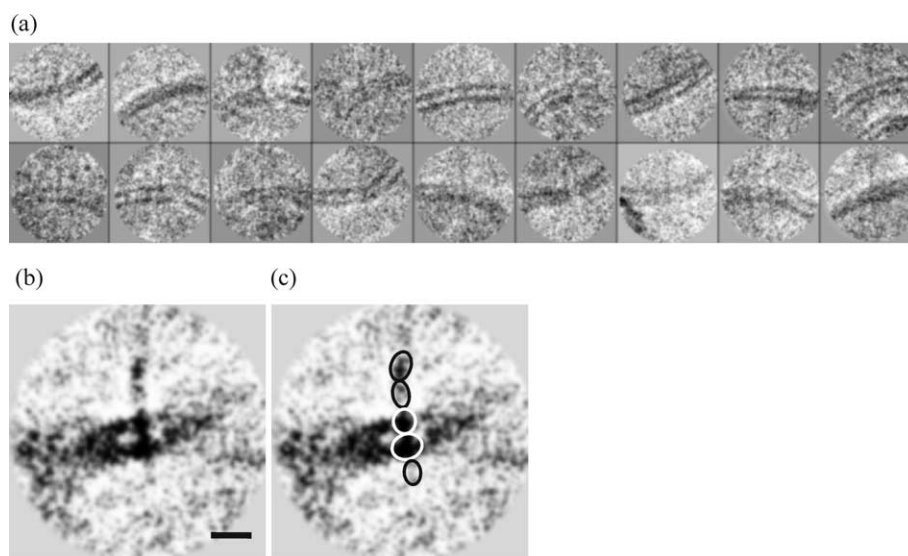


**Figure 4.** Individual images of PomA/B inserted into the lipid bilayers and two-dimensional average. (a) Individual images. (b) Two-dimensional average of those shown in (a). The bar represents 50 Å. (c) The same image as in (b), but overlaid with hypothetical domain envelopes.

from image to image, and conformations of the molecules appeared to have variations, 18 images (Figure 4(a)) were averaged roughly based on the manually picked points (see Materials and Methods). The resulting average is shown in Figure 4(b), and the hypothetical molecular envelope is drawn in Figure 4(c). The longer domain can be divided into two parts of similar dimension, a proximal and a distal domain. The density spanning the lipid bilayers shows an asymmetric distribution, and the one on the side of the shorter domain looks slightly larger than the other (Figure 4(c)), but this may be due to the clearly higher density contrast of the inner leaflet of the bilayers than the outer one (Figure 3). Although the shorter domain sticks out of the outer leaflet in the image shown in Figure 3(b), the orientation of the particle is opposite in 13 images out of 18 that were used to obtain the average, which puts the shorter domain on the side of inner leaflet in about two-thirds of the images. However, a different interpretation could be made based on the size of the cytoplasmic domains of PomA as described in Discussion. The size of the shorter domain in the average is smaller than those in individual raw images and probably due to its conformational variation.

### Gold-labeling

To ensure that the particles we observed above were the PomA/B complex, a gold label was introduced. PomB has three free cysteine residues, two in the N-terminal region (Cys10 and Cys8) and one in the transmembrane region (Cys31) (Figure 1(b)), whereas PomA has no cysteine. We used monomaleimido Nanogold with a 1.4 nm gold particle to label these cysteine residues. Because any

reductants would prevent the reaction and destroy gold particles, no reducing agent was added to the dialysis buffer. Under this condition, PomB forms a dimer with a disulfide bond as shown in the third and sixth lanes in Figure 2, but it is known that this bond formation does not affect the motor function of the motor.<sup>36</sup> An LI silver staining kit, which is a staining reagent specific for gold, was used to detect bound Nanogold as shown in the fourth lane in Figure 2. The band corresponding to the PomB dimer is clearly stained. The region corresponding to the smeared band of the PomA monomer and the region below are also stained, but these are probably due to non-specifically bound and unbound gold, respectively, as the stain density is much weaker compared to the amount of the protein shown in the third lane.

Individual gold particles are visible at relatively small defocus, e.g. at  $\sim 7000$  Å (Figure 5(a)), but are much harder to see at larger defocus, e.g. a few  $\mu\text{m}$ .<sup>42</sup> In contrast, proteins on the surface of liposomes can be barely seen at small defocus even by energy filtering (Figure 5(a)). Recording a pair of identical views at two different defocus levels seemed to be a good solution, but in practice the second shot frequently destroyed the lipid vesicles, particularly larger ones even at relatively low dose. Figure 5(b) shows the poor contrast of bound Nanogold in individual images recorded at a defocus of  $\sim 25,000$  Å. However, averaging of about ten images clearly revealed the bound gold particle, as shown in Figure 5(c). The density distribution of Nanogold is broad due to the rough alignment of heterogeneous images as described in Materials and Methods, Image analysis. Still, the high-density region is clearly located on the surface of the membrane on the shorter domain side. Since Cys31 is predicted to be located near the center of

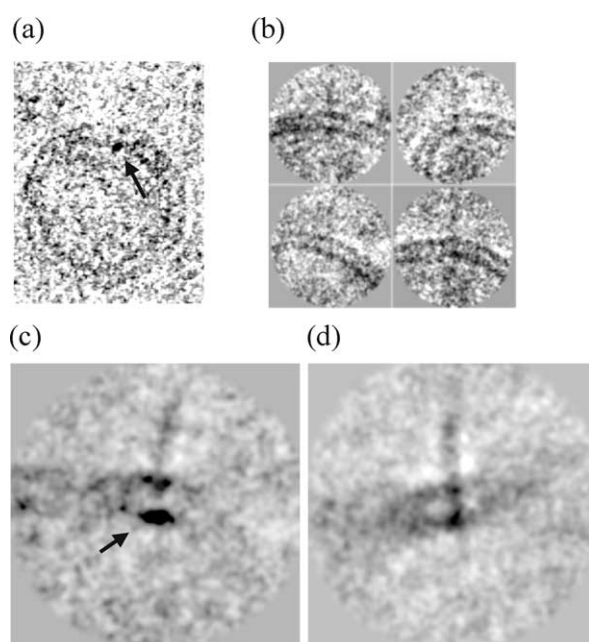


**Figure 5.** Individual and averaged images of PomA/B with bound Nanogold in comparison with the one without Nanogold labeling. (a) Image taken at a relatively small defocus level ( $\sim 7000$  Å underfocus). (b) Images taken at  $\sim 25,000$  Å underfocus. (c) Average of 12 images including those in (b). The contrast of the image is adjusted to show the peak corresponding to the averaged Nanogold density clearly. (d) The image without Nanogold, as already shown in Figure 4(b) but with its contrast adjusted to (c) for direct comparison. Arrows in (a) and (c) indicate a single bound Nanogold and the averaged density, respectively.

the membrane and not on the membrane surface (Figure 1(b)), this is not the one labeled. Since it is known that Cys31 is not responsible for the dimer formation,<sup>36</sup> either Cys8 or Cys10 must be forming a disulfide bond and the other labeled with Nanogold. Therefore, this result indicates that the side of the shorter domain is most likely the PomB N-terminal side.

### Deletion of peptidoglycan-binding motif

We also examined a mutant with deletion of the C-terminal 120 residues of PomB, which includes the peptidoglycan-binding motif (PomA/B $\Delta$ C).<sup>43</sup> This mutant protein was purified in the same way without any changes in the elution profile and the peak position in gel-filtration, despite the change in its molecular mass. The purified protein was reconstituted into liposomes in the same way. Although it was more difficult to find them in electron cryomicrographs because of the smaller size, we were able to record their images and averaged them in the same way as for the full-length protein complex. Figure 6 shows an average of 20 images. The particle does not have the large extramembrane domain, indicating that the side of the longer domain is most likely the periplasmic

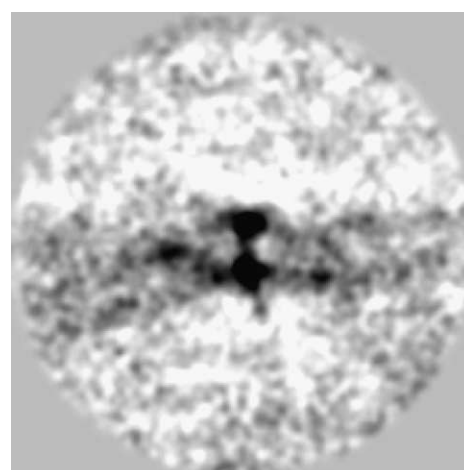


**Figure 6.** Average of 23 images of PomA/B $\Delta$ C.<sup>43</sup> The longer domain is missing.

side, where the peptidoglycan-binding domain of PomB is located.

## Discussion

Despite the important roles that PomA/B and MotA/B play in torque generation as the stator of the bacterial flagellar motor, even their overall shapes were not known. Here, we report the observation of the shape and domain arrangement of the PomA/B complex and locations of domains relative to the membrane bilayers, which was made possible by energy filtering electron cryomicroscopy of the purified complex reconstituted into liposomes.

Since conventional negatively stained or ice-embedded specimens of the purified complex dissolved in Chaps solutions did not show any structural features by electron microscopy, the complex was reconstituted into lipid vesicles, and the proteoliposomes embedded in vitreous ice were observed. A similar observation has been reported for a membrane protein, the low-density lipoprotein (LDL) receptor ( $\sim 115$  kDa), which has a large glycosylated extracellular domain and one trans-membrane helix,<sup>42</sup> but without energy filtering. Energy filtering can better resolve details of large samples such as liposomes embedded in relatively thick ice and produce images of higher amplitude contrast, because it removes inelastically scattered electrons, which otherwise give high background noise and increase as the specimen thickness increases. In particular, the phosphate head groups of lipids become distinctly clear (Figure 3(a)). Using energy filtering we were able to identify PomA/B clearly, even though its extramembrane regions are smaller than that of the LDL receptor.<sup>42</sup>

The images of liposomes with reconstituted PomA/B clearly resolved two extramembrane domains of different sizes sticking out of the lipid bilayers on opposite sides. The longer one is  $\sim 70$  Å long and the shorter one is roughly one-half of it.



A plasmid, pKJ301, which overproduces PomA/B with six histidine residues at the C terminus of PomB was used.<sup>37</sup> Purification of the PomA/B complex was carried out as described<sup>37</sup> with some modifications. Briefly, the membrane fraction was dissolved in 2.5% (w/v) Chaps, 20 mM Tris-HCl (pH 8.0), 150 mM KCl, 10% (v/v) glycerol, 1 tablet of Complete EDTA-free protease inhibitor cocktail (Roche Applied Science, Indianapolis, IN) and 20 mM imidazole (pH 8.0) at room temperature for 40 min. After the suspension was centrifuged at 100,000g for 30 min, the supernatant was applied to a column filled with Ni-NTA agarose (QIAGEN, Valencia, CA) and mixed at 4 °C for 1 h. Then, the column was washed with the same buffer except for containing 1% (w/v) Chaps. Then, the concentration of imidazole in the buffer was increased stepwise to 400 mM. PomA/B-His6 was well eluted at 50 mM–200 mM imidazole. The eluate was concentrated using a spin concentrator with a molecular mass cutoff of 10,000 Da and applied to a gel-filtration column, Superdex 200HR (Amersham Biosciences, Pittsburgh, PA). It was run at a flow rate of 0.5 ml/min in the same buffer but not containing imidazole. A fraction at the main peak corresponding to ~550 kDa was collected and subjected to the BCA assay (Pierce, Rockford, IL) for measurement of the protein concentration. Then, it was mixed with preformed liposomes made from *E. coli* polar lipid extract (Avanti Polar Lipids, Alabaster, AL) at a final concentration of the lipid of 1 mg/ml and a final ratio of protein to lipid of ~0.4 in the buffer containing 2% Chaps, and incubated at room temperature for 1 h. Then, the detergent was removed by dialysis against 20 mM Tris-HCl (pH 6.8) or 20 mM Mes (pH 6.5) (essential for gold labeling), 150 mM KCl, 10% (v/v) glycerol and 5 mM MgCl<sub>2</sub> at 37 °C overnight. PomB has free cysteine residues (Figure 1(b), white circles), whereas PomA has none. For gold labeling of cysteine, monomaleimido Nanogold with a 1.4 nm gold particle (Nanoprobes, Yaphank, NY) was added to the proteoliposomes at a final concentration of Nanogold at a few times excess to the protein, and the samples were incubated at room temperature for 1 h. Then, they were dialyzed again to remove unbound Nanogold at 4 °C for a few days. For SDS-PAGE, the samples were run on 12.5% or 15% (w/v) homogeneous polyacrylamide gel using the Laemmli buffer system.<sup>50</sup> To check monomaleimido Nanogold bound to the cysteine residues, the buffer system contained essentially no reductant. The gels were developed with an LI Silver stain kit (Nanoprobes, Yaphank, NY) to detect bound Nanogold. Western blot was done using anti-peptide antibodies against PomA and PomB.<sup>51</sup> We also examined a mutant PomA/B complex with deletion of the C-terminal 120 residues of PomB, which includes the peptidoglycan-binding motif. This mutant (PomA/BΔC) also has six histidine residues at its C terminus,<sup>43</sup> and therefore purification and preparation of its proteoliposomes were carried out as described above.

### Electron cryomicroscopy

A few microlitres of the proteoliposome solution was applied to a holey carbon grid and rapidly frozen in liquid ethane. These sample grids were mounted on an Oxford CT3500 cryo-holder (Gatan, Pleasanton, CA) and examined with a HITACHI EF-2000 electron microscope (Hitachi, Tokyo, Japan), equipped with a  $\gamma$ -type energy filter<sup>52</sup> and a cold field emission gun operated at an

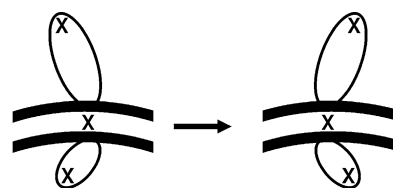


**Figure 8.** Schematic representation of the image alignment method. Three points (X) were marked manually at the tips of the longer and shorter extramembrane domains and at the center of the lipid bilayers. Some of the images were inverted into their mirror images about the axis approximately normal to the lipid bilayers (paired thick curves) for alignment and averaging.

accelerating voltage of 200 kV. An energy slit below the electromagnet was adjusted to select only electrons with energy loss less than 10 eV. Images were recorded on Kodak SO163 films (Eastman Kodak, Rochester, NY) at a nominal magnification of 70,000 $\times$  using a low-dose kit. Defocus levels of ~25,000 Å were used, which give the first zero of the contrast transfer function (CTF) at ~25 Å resolution.

### Image analysis

We selected by eye images that showed extramembrane domains sticking out of the lipid bilayers on both sides. The images were digitized with a LeafScan 45 linear CCD densitometer (LaserSoft Imaging, Longboat Key, FL) at a step size of 10  $\mu$ m. Magnification was calibrated with the layer-line spacing of the straight flagellar filaments<sup>53</sup> and the thickness of the lipid bilayers. Then, three points were manually marked on each PomA/B image, one on the longer and one on the shorter extramembrane domain and one on the center of the lipid bilayers, by using the SPIDER/WEB package.<sup>54</sup> Based on the selected points, each image was cut out into a small box and the density scales of the images were adjusted. Most of the PomA/B images were slightly curved in either one of two directions. To adjust relative positions of the three points among the images, some images were converted into their mirrored ones against a line approximately normal to the lipid plane (Figure 8). This procedure corresponds to the change of the direction of view or image projection by 180°. Then, all the images were aligned and averaged based on the two points on the longer and shorter domains. Since it was a manual-based alignment, to assure the reliability and reproducibility of the result, the whole procedure from marking points to the average was repeated three times to make sure the resulting 2D averages do not show any significant difference. The numbers of averaged images are 18 for the intact PomA/B complex, 12 for the one with gold labeling, and 23 for the deletion mutant.

### Acknowledgements

We thank Masaru Kojima for his help in harvesting bacteria and preparation of the membrane fraction, and Naoko Hattori for making deletion mutants.

## References

- Macnab, R. M. (2003). How bacteria assemble flagella. *Annu. Rev. Microbiol.* **57**, 77–100.
- Blair, D. F. (2003). Flagellar movement driven by proton translocation. *FEBS Letters*, **545**, 86–95.
- Yonekura, K., Maki-Yonekura, S. & Namba, K. (2002). Growth mechanism of the bacterial flagellar filament. *Res. Microbiol.* **153**, 191–197.
- Minamino, T. & Namba, K. (2004). Self-assembly and type III protein export of the bacterial flagellum. *J. Mol. Microbiol. Biotechnol.* **7**, 5–17.
- Dean, G. E., Macnab, R. M., Stader, J., Matsumura, P. & Burks, C. (1984). Gene sequence and predicted amino acid sequence of the motA protein, a membrane-associated protein required for flagellar rotation in *Escherichia coli*. *J. Bacteriol.* **159**, 991–999.
- Zhou, J., Fazio, R. T. & Blair, D. F. (1995). Membrane topology of the MotA protein of *Escherichia coli*. *J. Mol. Biol.* **251**, 237–242.
- Stader, J., Matsumura, P., Vacante, D., Dean, G. E. & Macnab, R. M. (1986). Nucleotide sequence of the *Escherichia coli* motB gene and site-limited incorporation of its product into the cytoplasmic membrane. *J. Bacteriol.* **166**, 244–252.
- Chun, S. Y. & Parkinson, J. S. (1988). Bacterial motility: membrane topology of the *Escherichia coli* MotB protein. *Science*, **239**, 276–278.
- Blair, D. F. & Berg, H. C. (1990). The MotA protein of *E. coli* is a proton-conducting component of the flagellar motor. *Cell*, **60**, 439–449.
- Stolz, B. & Berg, H. C. (1991). Evidence for interactions between MotA and MotB, torque-generating elements of the flagellar motor of *Escherichia coli*. *J. Bacteriol.* **173**, 7033–7037.
- Tang, H., Braun, T. F. & Blair, D. F. (1996). Motility protein complexes in the bacterial flagellar motor. *J. Mol. Biol.* **261**, 209–221.
- De Mot, R. & Vanderleyden, J. (1994). The C-terminal sequence conservation between OmpA-related outer membrane proteins and MotB suggests a common function in both Gram-positive and Gram-negative bacteria, possibly in the interaction of these domains with peptidoglycan. *Mol. Microbiol.* **12**, 333–334.
- Koebnik, R. (1995). Proposal for a peptidoglycan-associating alpha-helical motif in the C-terminal regions of some bacterial cell-surface proteins. *Mol. Microbiol.* **16**, 1269–1270.
- Coulton, J. W. & Murray, R. G. (1978). Cell envelope associations of *Aquaspirillum serpens* flagella. *J. Bacteriol.* **136**, 1037–1049.
- Khan, S., Dapice, M. & Reese, T. S. (1988). Effects of mot gene expression on the structure of the flagellar motor. *J. Mol. Biol.* **202**, 575–584.
- Socket, H., Yamaguchi, S., Kihara, M., Irikura, V. & Macnab, R. M. (1992). Molecular analysis of the flagellar switch protein FliM of *Salmonella typhimurium*. *J. Bacteriol.* **174**, 793–806.
- Irikura, V. M., Kihara, M., Yamaguchi, S., Socket, H. & Macnab, R. M. (1993). *Salmonella typhimurium* fliG and fliN mutations causing defects in assembly, rotation, and switching of the flagellar motor. *J. Bacteriol.* **175**, 802–810.
- Lloyd, S. A., Tang, H., Wang, X., Billings, S. & Blair, D. F. (1996). Torque generation in the flagellar motor of *Escherichia coli*: evidence of a direct role for FliG but not for FliM or FliN. *J. Bacteriol.* **178**, 223–231.
- Yorimitsu, T. & Homma, M. (2001). Na<sup>+</sup>-driven flagellar motor of *Vibrio*. *Biochim. Biophys. Acta*, **1505**, 82–93.
- McCarter, L. L. (2001). Polar flagellar motility of the *Vibrionaceae*. *Microbiol. Mol. Biol. Rev.* **65**, 445–462.
- Magariyama, Y., Sugiyama, S., Muramoto, K., Maekawa, Y., Kawagishi, I., Imae, Y. & Kudo, S. (1994). Very fast flagellar rotation. *Nature*, **371**, 752.
- Lowe, G., Meister, M. & Berg, H. C. (1987). Rapid rotation of flagellar bundles in swimming bacteria. *Nature*, **325**, 637–640.
- Chen, X. & Berg, H. C. (2000). Torque–speed relationship of the flagellar rotary motor of *Escherichia coli*. *Biophys. J.* **78**, 1036–1041.
- McCarter, L. L. (1994). MotY, a component of the sodium-type flagellar motor. *J. Bacteriol.* **176**, 4219–4225.
- McCarter, L. L. (1994). MotX, the channel component of the sodium-type flagellar motor. *J. Bacteriol.* **176**, 5988–5998.
- Gosink, K. K. & Häse, C. C. (2000). Requirements for conversion of the Na<sup>+</sup>-driven flagellar motor of *Vibrio cholerae* to the H<sup>+</sup>-driven motor of *Escherichia coli*. *J. Bacteriol.* **182**, 4234–4240.
- Okabe, M., Yakushi, T., Asai, Y. & Homma, M. (2001). Cloning and characterization of motX, a *Vibrio alginolyticus* sodium-driven flagellar motor gene. *J. Biochem.* **130**, 879–884.
- Okabe, M., Yakushi, T., Kojima, M. & Homma, M. (2002). MotX and MotY, specific components of the sodium-driven flagellar motor, colocalize to the outer membrane in *Vibrio alginolyticus*. *Mol. Microbiol.* **46**, 125–134.
- Okabe, M., Yakushi, T. & Homma, M. (2005). Interactions of MotX with MotY and with the PomA/PomB sodium ion channel complex of the *Vibrio alginolyticus* polar flagellum. *J. Biol. Chem.* **280**, 25659–25664.
- Sugiyama, S., Cragoe, E. J., Jr & Imae, Y. (1988). Amiloride, a specific inhibitor for the Na<sup>+</sup>-driven flagellar motors of alkalophilic *Bacillus*. *J. Biol. Chem.* **263**, 8215–8219.
- Atsumi, T., Sugiyama, S., Cragoe, E. J., Jr & Imae, Y. (1990). Specific inhibition of the Na<sup>+</sup>-driven flagellar motors of alkalophilic *Bacillus* strains by the amiloride analog phenamil. *J. Bacteriol.* **172**, 1634–1639.
- Asai, Y., Yakushi, T., Kawagishi, I. & Homma, M. (2003). Ion-coupling determinants of Na<sup>+</sup>-driven and H<sup>+</sup>-driven flagellar motors. *J. Mol. Biol.* **327**, 453–463.
- Sato, K. & Homma, M. (2000). Functional reconstitution of the Na<sup>+</sup>-driven polar flagellar motor component of *Vibrio alginolyticus*. *J. Biol. Chem.* **275**, 5718–5722.
- Braun, T. F. & Blair, D. F. (2001). Targeted disulfide cross-linking of the MotB protein of *Escherichia coli*: evidence for two H<sup>+</sup> channels in the stator complex. *Biochemistry*, **40**, 13051–13059.
- Kojima, S. & Blair, D. F. (2004). Solubilization and purification of the MotA/MotB complex of *Escherichia coli*. *Biochemistry*, **43**, 26–34.
- Yorimitsu, T., Kojima, M., Yakushi, T. & Homma, M. (2004). Multimeric structure of the PomA/PomB channel complex in the Na<sup>+</sup>-driven flagellar motor of *Vibrio alginolyticus*. *J. Biochem.* **135**, 43–51.
- Yakushi, T., Kojima, M. & Homma, M. (2004). Isolation of *Vibrio alginolyticus* sodium-driven flagellar motor complex composed of PomA and PomB solubilized by sucrose monopractate. *Microbiology*, **150**, 911–920.

38. Fukuoka, H., Yakushi, T., Kusumoto, A. & Homma, M. (2005). Assembly of motor proteins, PomA and PomB, in the Na<sup>+</sup>-driven stator of the flagellar motor. *J. Mol. Biol.* **351**, 707–717.
39. Smith, M. F. & Langmore, J. P. (1992). Quantitation of molecular densities by cryo-electron microscopy. Determination of the radial density distribution of tobacco mosaic virus. *J. Mol. Biol.* **226**, 763–774.
40. Zhu, J., Penczek, P. A., Schröder, R. & Frank, J. (1997). Three-dimensional reconstruction with contrast transfer function correction from energy-filtered cryoelectron micrographs: procedure and application to the 70 S *Escherichia coli* ribosome. *J. Struct. Biol.* **118**, 197–219.
41. Angert, I., Majorovits, E. & Schröder, R. R. (2000). Zero-loss image formation and modified contrast transfer theory in EFTEM. *Ultramicroscopy*, **81**, 203–222.
42. Jeon, H. & Shipley, G. G. (2000). Vesicle-reconstituted low density lipoprotein receptor. Visualization by cryoelectron microscopy. *J. Biol. Chem.* **275**, 30458–30464.
43. Yakushi, T., Hattori, N. & Homma, M. (2005). Deletion analysis of the carboxyl-terminal region of the PomB component of the *Vibrio alginolyticus* polar flagellar motor. *J. Bacteriol.* **187**, 778–784.
44. Francis, N. R., Sosinsky, G. E., Thomas, D. & DeRosier, D. J. (1994). Isolation, characterization and structure of bacterial flagellar motors containing the switch complex. *J. Mol. Biol.* **235**, 1261–1270.
45. Zhou, J. & Blair, D. F. (1997). Residues of the cytoplasmic domain of MotA essential for torque generation in the bacterial flagellar motor. *J. Mol. Biol.* **273**, 428–439.
46. Zhou, J., Lloyd, S. A. & Blair, D. F. (1998). Electrostatic interactions between rotor and stator in the bacterial flagellar motor. *Proc. Natl Acad. Sci. USA*, **95**, 6436–6441.
47. Yorimitsu, T., Sowa, Y., Ishijima, A., Yakushi, T. & Homma, M. (2002). The systematic substitutions around the conserved charged residues of the cytoplasmic loop of Na<sup>+</sup>-driven flagellar motor component PomA. *J. Mol. Biol.* **320**, 403–413.
48. Brown, P. N., Hill, C. P. & Blair, D. F. (2002). Crystal structure of the middle and C-terminal domains of the flagellar rotor protein FliG. *EMBO J.* **21**, 3225–3234.
49. Suzuki, H., Yonekura, K. & Namba, K. (2004). Structure of the rotor of the bacterial flagellar motor revealed by electron cryomicroscopy and single-particle image analysis. *J. Mol. Biol.* **337**, 105–113.
50. Laemmli, U. K. (1970). Cleavage of structural proteins during the assembly of the head of bacteriophage T4. *Nature*, **227**, 680–685.
51. Yorimitsu, T., Sato, K., Asai, Y., Kawagishi, I. & Homma, M. (1999). Functional interaction between PomA and PomB, the Na<sup>+</sup>-driven flagellar motor components of *Vibrio alginolyticus*. *J. Bacteriol.* **181**, 5103–5106.
52. Taya, S., Taniguchi, Y., Nakazawa, E. & Usukura, J. (1996). Development of  $\gamma$ -type energy filtering TEM. *J. Electron Microsc.* **45**, 307–313.
53. Maki-Yonekura, S., Yonekura, K. & Namba, K. (2003). Domain movements of HAP2 in the cap-filament complex formation and growth process of the bacterial flagellum. *Proc. Natl Acad. Sci. USA*, **100**, 15528–15533.
54. Frank, J., Radermacher, M., Penczek, P., Zhu, J., Li, Y., Ladjadj, M. & Leith, A. (1996). SPIDER and WEB processing and visualization of images in 3D electron microscopy and related fields. *J. Struct. Biol.* **116**, 190–199.

Edited by Sir A. Klug

(Received 13 September 2005; received in revised form 7 November 2005; accepted 9 December 2005)

Available online 4 January 2006